A continuous dynamic constitutive model for normal- and high-strength structural steels

Xiaoqiang Yang[a,b], Hua Yang[b,*], Leroy Gardner[c] and Yuyin Wang[b]

[a] College of Civil Engineering, Fuzhou University, Fuzhou, 350116, China

[b] School of Civil Engineering, Harbin Institute of Technology, Harbin, 150090, China

[c] Dept. of Civil and Environmental Engineering, Imperial College London, South Kensington Campus, London SW7 2AZ, UK

*Corresponding author. Postal address: Room 207, School of Civil Engineering, Harbin Institute of Technology, Huanghe Road #73, Nangang District, Harbin 150090, Heilongjiang Province, China.

Tel: +86 451 86282083

E-mail addresses: yanghua@hit.edu.cn

Abstract

The use of numerical models in the advanced analysis and design of steel structures, particularly under extreme loading conditions, is becoming increasingly widespread. A crucial component of such models is an accurate description of the material response. A systematic study into the dynamic constitutive modelling of structural steels is presented herein. The key features of the dynamic stress–strain characteristics of structural steels at various strain rates, i.e., test methods, material strength, strain-rate effect index and strain-rate effect models, are examined and discussed. Supplementary SHPB tests on both normal- and high-strength structural steels (Q235, Q355, Q460, and S960) under a wide range of strain rates up to 5000 s^{-1}, filling gaps in existing datasets, are then carried out. A database of dynamic test results, containing 453 stress–strain curves, is systematically established and analyzed. Finally, a continuous dynamic constitutive model, capturing the dependency of both yield strength and strain rate, is proposed to predict the dynamic stress–strain response for structural steels, from normal- to high-strength material (235–960 MPa), and from static to high strain rate loading conditions (up to 5000 s^{-1}).

Keywords: strain rate, strain-rate effect, high-strength structural steel, dynamic test, dynamic constitutive model, stress–strain curves.

1 Introduction

There is a growing demand for modern infrastructure to be resilient to extreme events, such as earthquakes, vehicle impacts, and explosions. The effective simulation of steel structures under the dynamic loading conditions that arise from such extreme events requires an accurate description of the material stress–strain response, including the influence of strain rate effects [1]. At the same time, there is increasing use of high-strength steel [2-4] in the construction industry, prompting the need for a dynamic constitutive model that is applicable across a broad range of steel grades.

Since the middle of the twentieth century, a number of studies [5-8] into the dynamic behaviour of mild steels have been carried out, identifying and quantifying the importance of strain-rate effects on the dynamic yield and ultimate strengths. Recently, the strain rate-dependent properties of normal-strength [9-17] and high-strength [15, 17-23] structural steels have been investigated at intermediate and high strain rates, and full dynamic stress–strain curves have been obtained and analyzed. Several strain-rate effect models have also been developed to predict the dynamic properties of specific steel grades. However, some limitations in these models exist: (1) there is typically a narrow testing range for both steel grade and strain rate, (2) the adopted strain-rate effect indices are not always appropriate, and (3) constitutive models are only available for a limited number of steel grades. These issues are discussed further in Section 2, and addressed in this study.

This paper first presented a comprehensive discussion on the previous studies into the dynamic stress–strain properties of structural steels. Supplementary tests for normal- and high-strength structural steels were then conducted to fill the gaps (i.e., high-strength steels and high strain rates) in existing datasets. A continuous dynamic constitutive model was established with a broad range of nominal yield strengths (235-960 MPa) under static to high strain rates (≤5000 s^{-1}), based on the database of relevant available test results.

2 Previous studies into dynamic properties of structural steels

Table 1 summarizes previous studies into the dynamic stress–strain characteristics of structural steels [6, 9-23], where the key information with respect to the studied steel grades, numbers of tests, adopted strain rates, data processing method and test setup is provided. Some early studies [5, 7, 8], in which full stress–strain curves were not reported, have been excluded from Table 1, while the particular steel grades used in the WTC [17] were not specifically reported.

Table 1 Summary of dynamic tests on structural steels.

Series	No.	Grades	f_y / MPa	Groups	Repeated tests	$\dot{\varepsilon}$ /s^{-1}	Method of defining $f_{y,d}$	Test setups	References
	1	A36	262	4	3	0.01-12.2	Lower & upper yield strength	High-speed MTS	Cowell (1969) [6]
	2	A242 (Flat)	411	4	3	0.01-12.4	Lower & upper yield strength	High-speed MTS	Cowell (1969) [6]
	3	A242 (Round)	339	4	3	0.01-14.2	Lower & upper yield strength	High-speed MTS	Cowell (1969) [6]
	4	A441	338	4	3	0.01-12.2	Lower & upper yield strength	High-speed MTS	Cowell (1969) [6]
	5	A572	365	4	3	0.01-12.6	Lower & upper yield strength	High-speed MTS	Cowell (1969) [6]
	6	St52-3N	358, 400	10	2	0.01-1095	Lower & upper yield strength	SHTB	Langseth et al. (1991) [9]
Normal-strength	7	AS3678	342	2	n.a.	1, 10	0.2% offset	High-speed MTS	Mirmomeni et al. (2015) [10]
	8	Q345	374	4	3	500-4000	n.a.	SHPB	Yu et al. (2010) [11]
	9	Q235	321	6	3	4.4-315	Average yield strength	High-speed tensile machine	Chen et al. (2016) [12]
	10	Q345	372	6	3	0.1-330	Average yield strength	High-speed tensile machine	Chen et al. (2017) [13]
	11	Q420	436	6	3	0.1-288	Average yield strength	High-speed tensile machine	Chen et al. (2017) [14]
	12	S235	235	4	3	0.04-4	0.2% offset	Instron & dynamic machine	Alabi et al. (2018) [15]
	13	S355	441	5	3	5-850	0.2% offset	SHTB	Forni et al. (2016) [16]
	14-1	Steels in WTC	256-436	29	n.a.	63-417	1% offset	High-speed tensile machine	Luecke et al. (2005) [17]
	14-2	Steels in WTC	463-789	36	n.a.	54-515	1% offset	High-speed tensile machine	Luecke et al. (2005) [17]
	15	S690	817	4	3	0.04-4	0.2% offset	Instron & dynamic machine	Alabi et al. (2018) [15]
	16	S960	906	4	3	0.04-4	0.2% offset	Instron & dynamic machine	Alabi et al. (2018) [15]
High-strength	17	S960	973, 1024	6	3	250-950	0.2% offset	SHTB	Cadoni and Forni (2019) [18]
	18	S690	775, 808	10	3	3-950	0.2% offset	Hydro-pneumatic machine & SHTB	Cadoni and Forni (2020) [19]
	19	Q550	624	5	3	540-3831	0.2% offset	SHPB	Yang et al. [20]
	20	S690	722	12	3	0.1-4109	0.2% offset	High-speed tensile machine, SHPB	Yang et al. [21, 22]
	21	S890	924	8	3	0.1-5293	0.2% offset	High-speed tensile machine, SHPB	Zhu et al. [23]
	22	Q235	274	6	3	600-5194	0.2% offset	SHPB	
Normal- & high-strength	23	Q355	416	6	3	269-4803	0.2% offset	SHPB	Present study
	24	Q460	484	5	3	849-4562	0.2% offset	SHPB	
	25	S960	952	5	3	890-4142	0.2% offset	SHPB	
Summary		**16 Grades**	**235-1024**	**199**		**0.01-5293**	**4 methods**	**4 devices**	**16 references and present study**

Note: f_y is the static yield strength; $\dot{\varepsilon}$ is the applied strain rate; $f_{y,d}$ is the dynamic yield strength.

2.1 Test methods for different strain rates

Structures can experience a wide range of different strain rates depending on the type of loading to which they are subjected. Based on [21], a typical classification of strain rates in terms of the magnitude, i.e., static, quasi-static, intermediate and high strain rates, is depicted in Fig. 1. Acquiring test data across this very wide range of strain rates, requires the use of a number of different experimental dynamic testing techniques. For static and quasi-static strain rates, servo-hydraulic universal testing machines are generally employed, with a typical maximum strain rate of 10^{-2} s^{-1}. For intermediate and high strain rates, high-speed testing machines (typically suitable in the 10^{-2}–10^{2} s^{-1} strain-rate range), and split Hopkinson pressure or tensile bars (SHPB or SHTB) for strain rates higher than 10^{2} s^{-1}, respectively, are generally employed (see Fig. 1). The reliability and consistency of test results can vary between the different experimental techniques with variability typically increasing with increasing strain rate [19, 21-23].

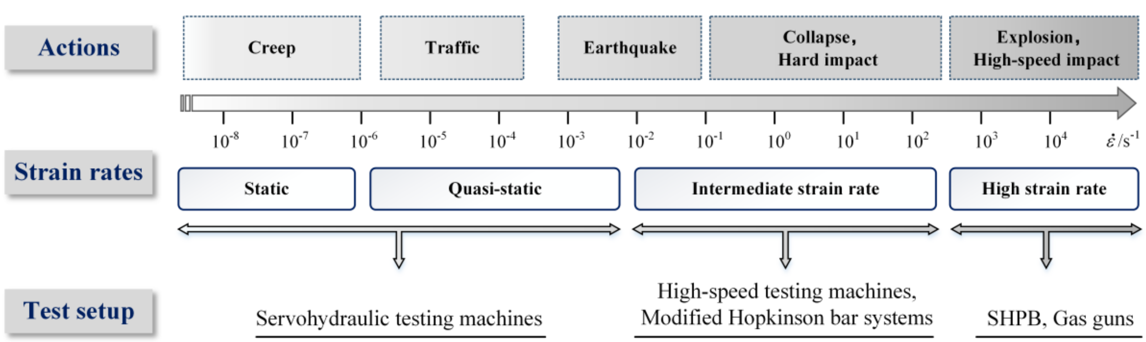

Fig. 1 Typical classification of strain rates [21].

2.2 Strain-rate effect indices

Three indices are commonly used to quantify strain-rate effects in structural steels: DIF_y is the dynamic increase factor for the yield strength, defined as the ratio of the dynamic yield strength $f_{y,d}$ to the static yield strength f_y, i.e., $DIF_y = f_{y,d} / f_y$ (see Fig. 2a); DIF_u is the dynamic increase factor for the ultimate strength, defined as the ratio of the dynamic ultimate strength $f_{u,d}$ to the static ultimate strength f_u, i.e., $DIF_u = f_{u,d} / f_u$ (see Fig. 2a); and DIF_{avg} is the average dynamic increase factor of the full dynamic true stress (σ_{true})-true plastic strain ($\varepsilon_{true,pl}$) curve, which is defined as follows. Dividing the dynamic stress ($\sigma_{i,d}$) by the quasi-static stress ($\sigma_{i,s}$), DIF_i can be determined at defined strain intervals from the yield point ($DIF_i = \sigma_{i,d} / \sigma_{i,s}$, where i is the number of strain intervals). At each strain rate, the relationship between DIF_i and $\varepsilon_{true,pl}$ is obtained, and the DIF_{avg} can be calculated by averaging the obtained DIF_i values, i.e., $DIF_{avg} = \Sigma DIF_i / i$ (see Fig. 2b).

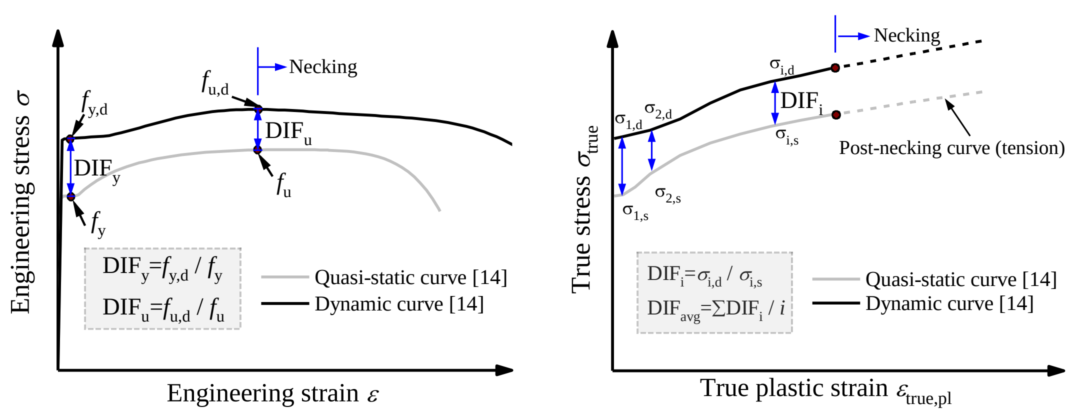

(a) DIF_y and DIF_u (b) DIF_{avg}

Fig. 2 Definition of strain-rate effect indices.

Among the three indices, DIF_y is widely used, but can result in somewhat inaccurate predictions if applied as a stress amplification factor to the full quasi-static stress–strain curve for the following reasons: (i) when subjected to impact or explosion, steel typically deforms into the strain-hardening range, which is far beyond the yield point; (ii) the dynamic increment in $f_{y,d}$ is generally higher than that of other points on the stress–strain curve, leading to an overestimation of the predicted constitutive response when using DIF_y; (iii) measured DIF_y values reported in the literature can be sensitive to the system errors associated with stress nonuniformity during the elastic stage in SHPB tests, and to the various methods of defining $f_{y,d}$ for those steels with a yield plateau (e.g., lower/upper yield strength [6] or average yield strength [12-14]) and those without a yield plateau (e.g., 0.2% proof strength [10, 15, 16, 18], and 1% proof strength [17]). Thus, DIF_y is often not the most suitable or consistent means of characterizing the dynamic properties of structural steels.

Use of the dynamic increase factor for the ultimate strength DIF_u also has a number of limitations: (i) it is not possible to determine DIF_u through SHPB compressive tests at high strain rates, since the compressive stress continues to increase with increasing compressive strain (i.e., without exhibiting a peak), often resulting in the absence of DIF_u values in existing datasets at high strain rates, and (ii) the magnitude of DIF_u is generally lower than that of DIF_y for a given strain rate [13, 14, 21], leading to an underestimation of the predicted constitutive response when applied to the full stress-strain curve.

In light of the shortcomings of using the yield or ultimate dynamic increase factors, the average dynamic increase factor DIF_{avg}, previously proposed by the authors [21, 22], is considered to be the most suitable and representative means of describing the strain rate dependency of the post-yield constitutive response of steels. Hence, DIF_{avg} is the key parameter employed in this study to establish the dynamic stress–strain model.

2.3 Existing strain-rate effect models

Several strain-rate effect models for predicting the dynamic properties of steel have been proposed in the literature [26-31]. Among the developed models, the Cowper-Symonds (C-S) [28] and Johnson-Cook (J-C) [29] models, expressed by Eq. (1) and Eq. (2), respectively, are the most widely used because of their relatively high prediction accuracy and simple, intuitive forms:

$$\frac{\sigma}{\sigma_{\mathrm{s}}} = 1 + \left(\frac{\dot{\varepsilon}}{D}\right)^{\frac{1}{p}} \tag{1}$$

$$\sigma = \left(A + B{\varepsilon_{\mathrm{p}}}^{n}\right)(1 + Cln\varepsilon^{*})(1 - T^{*m}) \tag{2}$$

where σ and σ_{s} are the dynamic and static stresses, ε_{p} is the plastic strain, $\dot{\varepsilon}$ is the strain rate, $\varepsilon^{*} = \dot{\varepsilon}/\varepsilon_0$, ε_0 is the reference strain rate, $T^{*} = (T - T_{\mathrm{r}})/(T_{\mathrm{m}} - T_{\mathrm{r}})$, in which T is the test temperature, T_{r} is the room temperature and T_{m} is the melting temperature, and D, p, A, B, C, m, and n are material constants. These models can also be directly applied within commercial finite element packages, such as ABAQUS [32] and ANSYS [33].

Strain rate sensitivity is generally accepted to the dependent on the material strength, with high-strength steel being less sensitive than normal-strength steel. For example, the average measured dynamic increase factors (DIF_{avg}) of the Q345 steel tested in [13] were 1.12 and 1.44 at strain rates of 0.1 s^{-1} and 200 s^{-1}, respectively, while the corresponding DIF_{avg} values for the S690 steel tested in [21] were 1.05 and 1.18, respectively. Hence, both the C-S and J-C models, have been calibrated in previous research [12-14, 16, 18, 20-23] to predict the dynamic properties of different steels through different material coefficients. This has inevitably led to a series of discrete models applicable to individual steel grades, as shown in Fig. 3. These discrete models, often fitted to a relatively small number of test results, generally lack continuity between grades. Hence, a continuous model to predict full dynamic stress–strain curves, which is applicable across a wide range of steel grades and strain-rate ranges, is sought herein.

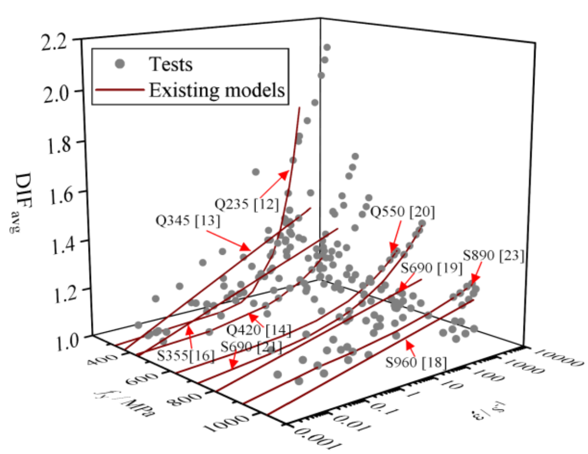

Fig. 3 General view of existing discrete strain-rate models, together with assembled test data discussed in Section 3.2.

3 Tests and database

3.1 Test program

An experimental investigation into the stress–strain responses of normal- and high-strength steel (grades Q235, Q355, Q460 and S960) at quasi-static and high strain rates, is described in this section to fill gaps in the existing datasets. The quasi-static tests were performed using an electromechanical universal testing machine (Fig. 4a), while the high strain rate tests were carried out using an SHPB setup (Fig. 4b). Traditional dog-bone coupons were employed for the quasi-static tests with a strain rate of 0.00025 s^{-1}, in accordance with ISO 6892-1:2016. All the specimens for the SHPB tests were cylinders, each with a diameter of 8 mm and a length of 4 mm. Five or six groups for each steel with different gas pressure magnitudes (to obtain various strain rates) were designed to assess the behaviour across a range of high strain rates, where the average strain rate was defined as the representative strain rate for each group. The testing procedures and data processing methods are the same as those utilized in previous studies by the authors [20-23].

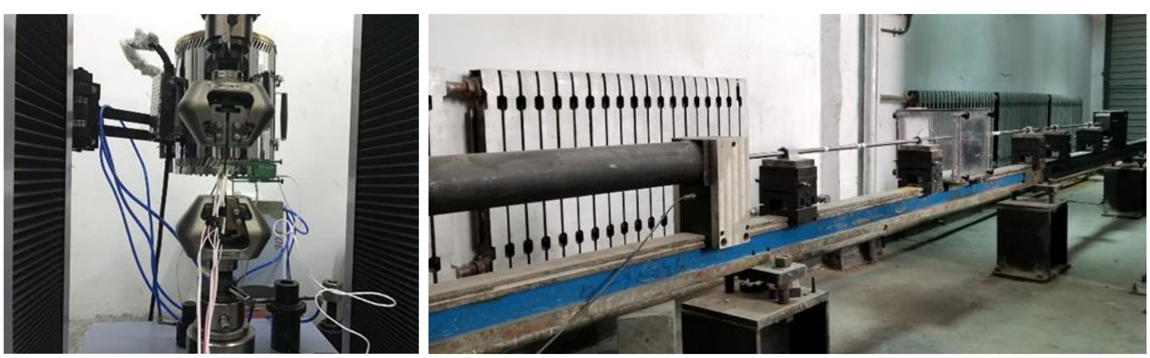

(a) Universal testing machine (b) SHPB

Fig. 4 Testing system.

The three stress–strain curves of the repeat quasi-static coupon tests are plotted for each steel grade in Fig. 5; the results of the repeat tests are highly consistent, and the average curves are also shown. With increasing yield strength, the measured stress-strain curves exhibited shorter yield plateau lengths, less strain-hardening and reduced ultimate strains. The measured quasi-static properties of the steels are listed in Table 2. Note that the yield strength of the S960 steel was defined using the 0.2% offset method since no well-defined yield point was observed.

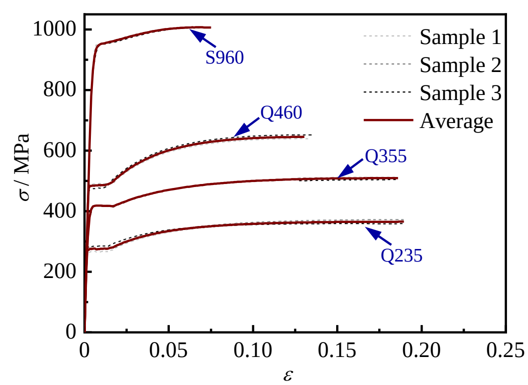

Fig. 5 Engineering stress–strain curves obtained from uniaxial quasi-static tension tests on studied steel grades.

Table 2 Tensile properties of different steels obtained from uniaxial quasi-static coupon tests.

Grade	f_y / MPa	f_u / MPa	ε_u	f_u/f_y	E_s / ×10^5MPa	Possion's Ratio
Q235	274	366	0.19	1.34	2.00	0.296
Q355	416	509	0.18	1.22	2.01	0.268
Q460	484	645	0.13	1.33	2.01	0.283
S960	952	1007	0.07	1.06	2.05	0.293

Note: f_y is the yield strength, f_u is the ultimate strength, ε_u is the strain when the ultimate strength is reached, and E_s is Young's modulus.

Fig. 6 shows four groups of typically measured engineering stress–strain curves from repeat SHPB tests, and high consistency is observed. The average curves for all steels are calculated based on the three repeat tests, as shown in Fig 7. Significant strain-rate effects can be observed for all studied grades. It should be noticed that the stress uniformity is not satisfied entirely at the early stage of SHPB tests, and wave dispersion, inertia effect, and surface friction cannot be completely eliminated, which leads to the oscillation of dynamic stress [20, 22]. Hence, the elastic section of dynamic curves is unreliable, and the wave shapes in the dynamic curves are observed, especially for high strain rates. That also makes it difficult to define the dynamic yield strength using the common 0.2% offset method. According to the previous studies [22, 34], by removing the elastic section of the engineering stress–strain curve and linearly fitting the strain-strengthening section, the intersection point between the linearly fitted line and 0.2% offset trend line (based on quasi-static Young's modulus and 0.2% residual strain) can be defined as the dynamic yield strength (see Fig. 8).

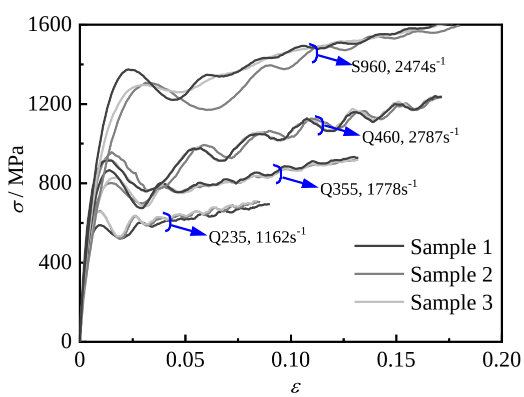

Fig. 6 Measured engineering stress–strain curves for typical repeat tests.

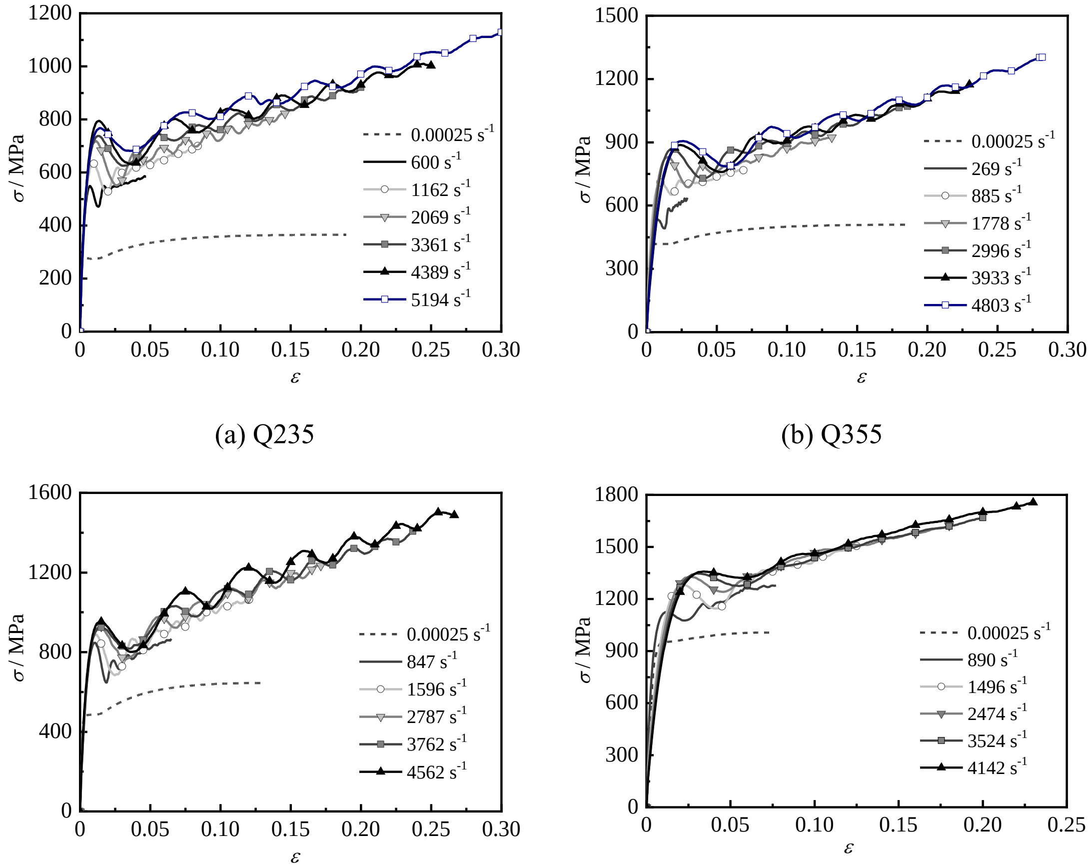

(a) Q235 (b) Q355

(c) Q460 (d) S960

Fig. 7 Engineering stress–strain curves of each steel at different strain rates.

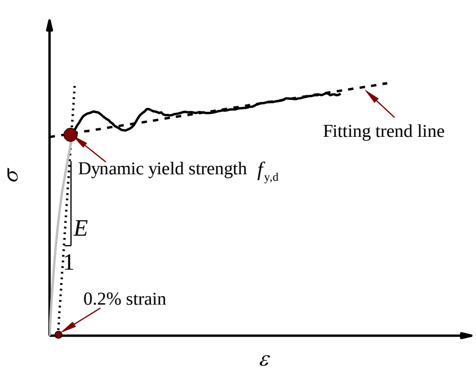

Fig. 8 Definition of dynamic yield strength [22].

The engineering stress and engineering strain were converted into the true stress σ_{true} and true strain $\varepsilon_{\text{true}}$ using Eqs (3) and (4) to obtain the true stress–strain curves.

$$\sigma_{\text{true}} = (1+\varepsilon)\sigma \quad (3)$$

$$\varepsilon_{\text{true}} = ln(1+\varepsilon) \quad (4)$$

where σ and ε are the engineering stress and engineering strain, respectively.

Subsequently, the true plastic strain $\varepsilon_{\text{true,pl}}$ was determined by removing the elastic strain component, obtaining the true stress–true plastic strain curves, as plotted in Fig. 9. The plastic flow stress of each steel grade showed evident strain-rate sensitivity. Using the measured dynamic stress–strain curves (Figs 7 and 9), the DIF_y and DIF_{avg} values were determined for all considered steel grades and strain rates, as listed in Table 3. It can be seen that the DIF_y can be up to 20% higher than DIF_{avg} at high strain rates, confirming the limitations of using DIF_y values for representing the strain-rate effect over the full range of the stress–strain curves, as mentioned in Section 2.2. The dynamic curves at higher strain rates are longer than those at lower strain rates. This is because to produce a higher strain rate, the higher impact energy of the strike bar (i.e., larger gas pressure) is essentially needed during the SHPB test. It also results in more compression deformation of the specimen, and the end strain will be enlarged when tests are completed. It should be noticed that the end strain is not the nominal ultimate strain, as the dynamic compressive stress is typically increased as the strain increases without a peak value.

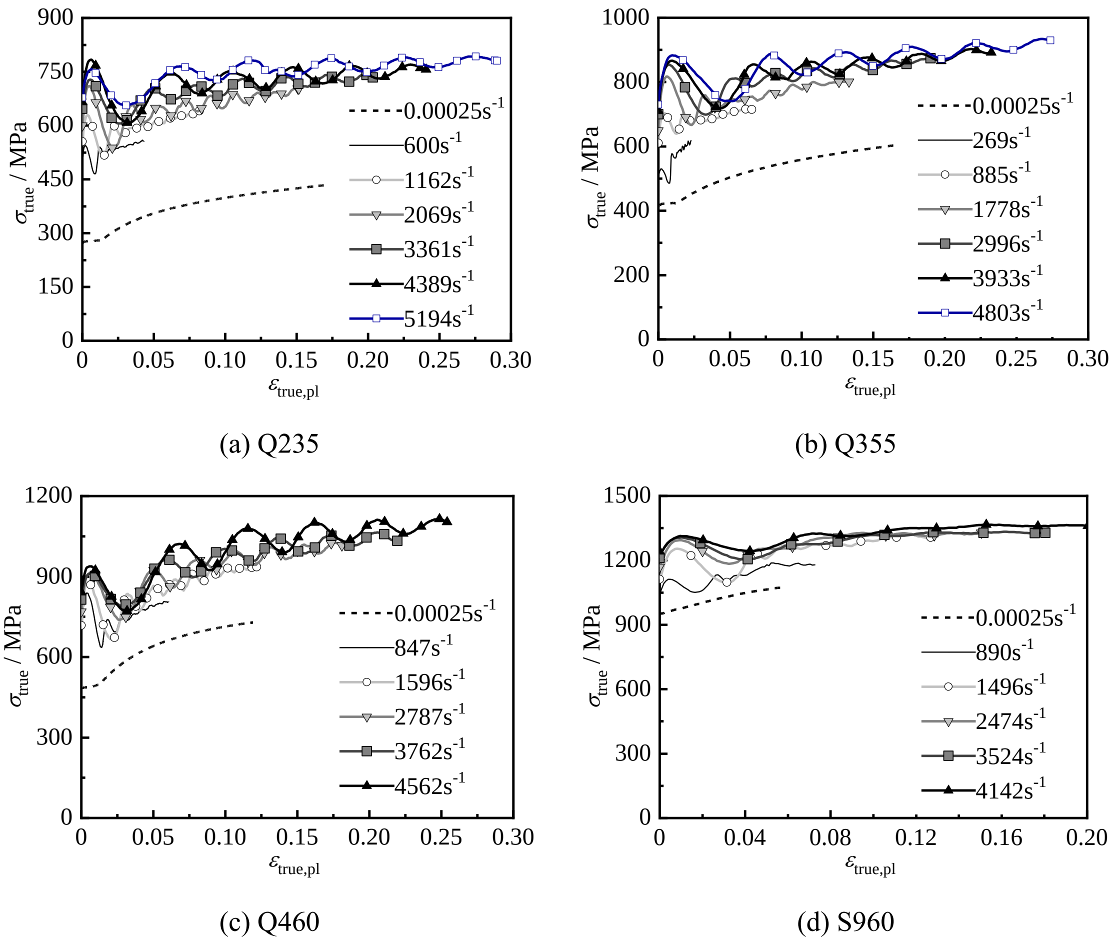

Fig. 9 True stress-true plastic strain curves of each steel at different strain rates.

Table 3 Summary of test results for different steels.

Grade	$\dot{\varepsilon}$ / s^{-1}	$f_{y,d}$ / MPa	DIF$_y$	DIF$_{avg}$	Grade	$\dot{\varepsilon}$ / s^{-1}	$f_{y,d}$ / MPa	DIF$_y$	DIF$_{avg}$
Q235	600	508	1.854	1.688	Q355	269	558	1.341	1.225
	1162	555	2.026	1.773		885	650	1.563	1.405
	2069	600	2.190	1.848		1778	690	1.659	1.466
	3361	647	2.361	1.964		2996	720	1.731	1.548
	4389	665	2.427	2.030		3933	740	1.779	1.584
	5194	678	2.474	2.084		4803	753	1.810	1.631
Q460	847	671	1.386	1.265	S960	890	1060	1.113	1.093
	1596	718	1.483	1.344		1496	1120	1.176	1.151
	2787	770	1.591	1.397		2474	1178	1.237	1.167
	3762	814	1.682	1.426		3524	1216	1.277	1.187
	4562	842	1.740	1.463		4142	1242	1.305	1.203

3.2 Establishment of database

A total of 453 experimental dynamic stress-strain curves have been collected from the present study and 16 sources from the literature [6, 9-23] and analysed. Considering repeat tests as a single data point, a database comprising a total of 199 independent data points (i.e., DIF values) was assembled, as shown in Table 1. The parameter ranges of the entire database were 235 MPa $\leq f_y \leq$ 1024 MPa and 0.001 s^{-1} $\leq \dot{\varepsilon} \leq$ 5000 s^{-1}.

The distribution of the assembled dynamic tests, in terms of yield strength and strain rate, is illustrated in Fig. 10. It can be seen that, after the introduction of the authors' test results ([20-23] and the present study), the coverage of the data is more comprehensive (see Fig. 10b), providing a sound basis for the establishment of dynamic constitutive models. As shown in Fig. 11, the assembled DIF_{avg} data show a clear dependency on both strain rate and steel strength.

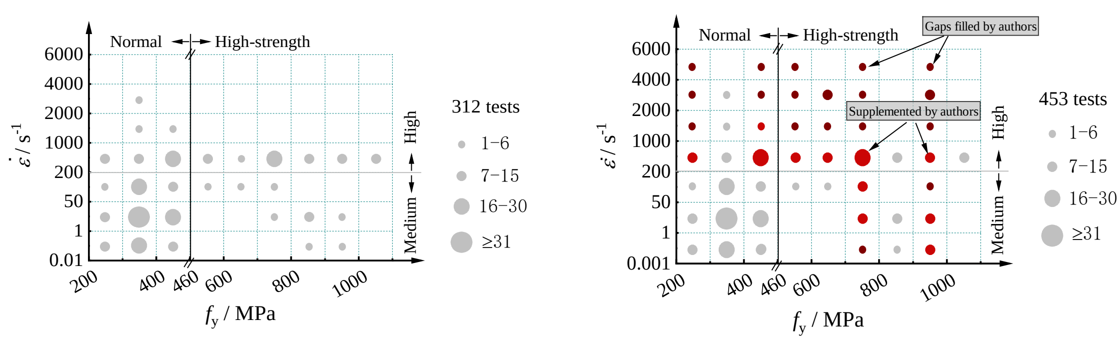

(a) Existing tests from other researchers (b) Existing plus author tests

Fig. 10 Distributions of dynamic material tests on structural steels.

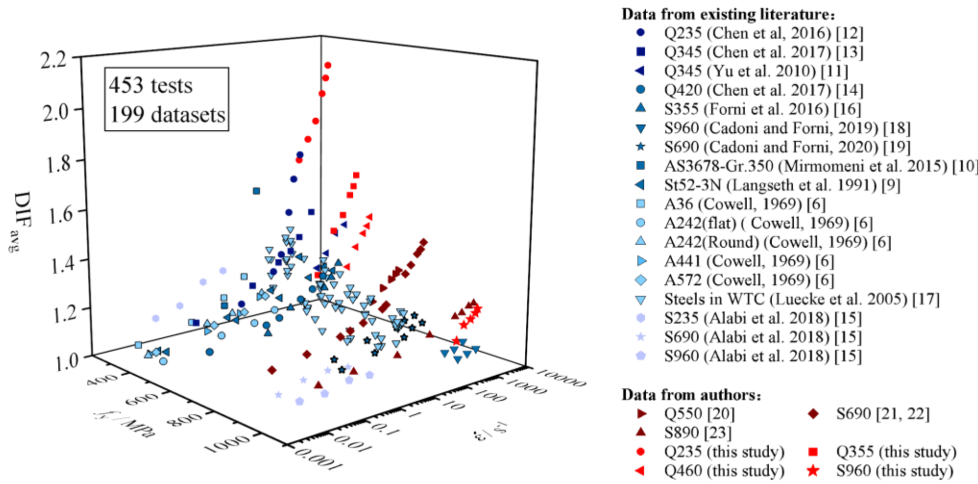

Fig. 11 Database of $\mathrm{DIF}_{\mathrm{avg}}$ values for structural steels.

4 Proposed dynamic constitutive model

Based on the established database, a continuous dynamic constitutive model for structural steels is proposed in this section, using an average dynamic increase factor to multiply the static stress-strain curve, as expressed by Eq. (5). In this equation, $\sigma_{\mathrm{s}}(\varepsilon)$ is the static stress-strain curve, which is carefully discussed in Section 4.1; $\mathrm{DIF}_{\mathrm{avg}}(\dot{\varepsilon}, f_{\mathrm{y}})$ is a proposed strain-rate effect model developed in Section 4.2.

$$\sigma = \sigma_{\mathrm{s}}(\varepsilon) \cdot \mathrm{DIF}_{\mathrm{avg}}(\dot{\varepsilon}, f_{\mathrm{y}}) \tag{5}$$

4.1 Static stress–strain relationship

The static stress–strain curve of the steel serves as the basis for determining the dynamic stress–strain curve. The static stress–strain curve may be established either directly through physical testing or from existing constitutive models. To represent the full range engineering stress–strain response of hot-rolled steels, which are the focus of the present study, the constitutive models developed by Yun and Gardner [35], as given below, are recommended. The first model, given by Eq. (6) and illustrated in Fig. 12, describes a quad-linear stress–strain response, while the second, given by Eq. (7) and illustrated in Fig. 13, describes a bi-linear plus nonlinear hardening stress–strain response. Both models were calibrated against a large set of experimental stress–strain curves. The only difference between the models is in the form of the strain hardening region.

$$\sigma = \begin{cases} E\varepsilon & \varepsilon \le \varepsilon_{\mathrm{y}} \\ f_{\mathrm{y}} & \varepsilon_{\mathrm{y}} < \varepsilon \le \varepsilon_{\mathrm{sh}} \\ f_{\mathrm{y}} + E_{\mathrm{sh}}(\varepsilon - \varepsilon_{\mathrm{sh}}) & \varepsilon_{\mathrm{sh}} < \varepsilon < \mathrm{C}_1\varepsilon_{\mathrm{u}} \\ f_{\mathrm{C}_1\varepsilon_{\mathrm{u}}} + \frac{f_{\mathrm{u}} - f_{\mathrm{C}_1\varepsilon_{\mathrm{u}}}}{\varepsilon_{\mathrm{u}} - \mathrm{C}_1\varepsilon_{\mathrm{u}}}(\varepsilon - \varepsilon_{\mathrm{sh}}) & \mathrm{C}_1\varepsilon_{\mathrm{u}} < \varepsilon < \varepsilon_{\mathrm{u}} \end{cases} \quad (6)$$

$$\sigma = \begin{cases} E\varepsilon & \varepsilon \le \varepsilon_{\mathrm{y}} \\ f_{\mathrm{y}} & \varepsilon_{\mathrm{y}} < \varepsilon \le \varepsilon_{\mathrm{sh}} \\ f_{\mathrm{y}} + (f_{\mathrm{u}} - f_{\mathrm{y}})\left\{0.4\varepsilon^* + \frac{2\varepsilon^*}{[1+400(\varepsilon^*)^5]^{0.2}}\right\} & \varepsilon_{\mathrm{sh}} < \varepsilon < \varepsilon_{\mathrm{u}} \end{cases} \quad (7)$$

where σ and ε are the stress and strain, respectively, f_{y}, f_{u}, and E are the yield strength, ultimate strength and Young's modulus, respectively, and ε^* is defined as:

$$\varepsilon^* = \frac{\varepsilon - \varepsilon_{\mathrm{sh}}}{\varepsilon_{\mathrm{u}} - \varepsilon_{\mathrm{sh}}}, \quad (8)$$

with the ultimate strain ε_{u} given by:

$$\varepsilon_{\mathrm{u}} = 0.6\left(1 - \frac{f_{\mathrm{y}}}{f_{\mathrm{u}}}\right), \text{ but } \varepsilon_{\mathrm{u}} \ge 0.06 \text{ for hot-rolled steels,} \quad (9)$$

and the strain hardening strain $\varepsilon_{\mathrm{sh}}$ given by:

$$\varepsilon_{\mathrm{sh}} = 0.1\frac{f_{\mathrm{y}}}{f_{\mathrm{u}}} - 0.055, \text{ but } 0.015 \le \varepsilon_{\mathrm{sh}} \le 0.03, \quad (10)$$

The material coefficient C_1 is determined from

$$\mathrm{C}_1 = \frac{\varepsilon_{\mathrm{sh}} + 0.25(\varepsilon_{\mathrm{u}} - \varepsilon_{\mathrm{sh}})}{\varepsilon_{\mathrm{u}}}, \quad (11)$$

while the slope of the strain hardening region E_{sh} is given by:

$$E_{\mathrm{sh}} = \frac{f_{\mathrm{u}} - f_{\mathrm{y}}}{0.4(\varepsilon_{\mathrm{u}} - \varepsilon_{\mathrm{sh}})}. \tag{12}$$

Note that the above stress–strain relationships both feature a yield plateau, though this does not always appear for high-strength steels, in which case, a bilinear elastic linear hardening model or a rounded stress–strain model [36, 37] may be used, as illustrated in Figs 14 and 15, respectively. Based on the test results obtained by the authors on the S690 high-strength steels [21, 22], a suitable value for the slope of the strain hardening region is E_{sh}=0.003E_{s}.

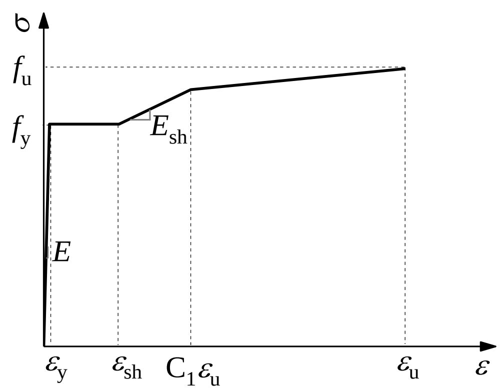

Fig. 12 Quad-linear stress-strain model for hot-rolled steels.

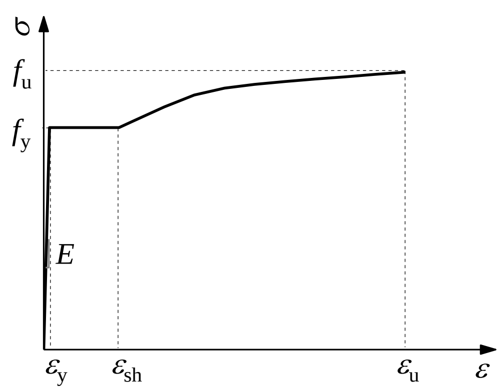

Fig. 13 Bilinear plus nonlinear hardening stress-strain model for hot-rolled steels.

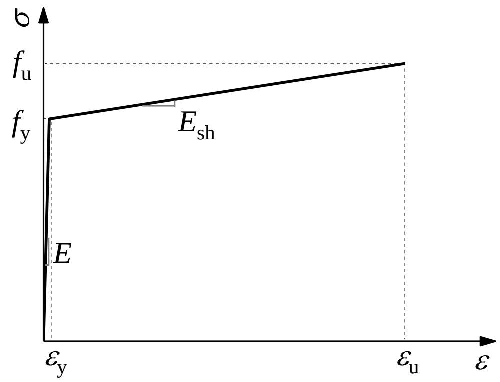

Fig. 14 Bilinear elastic linear hardening stress-strain model for high-strength steel.

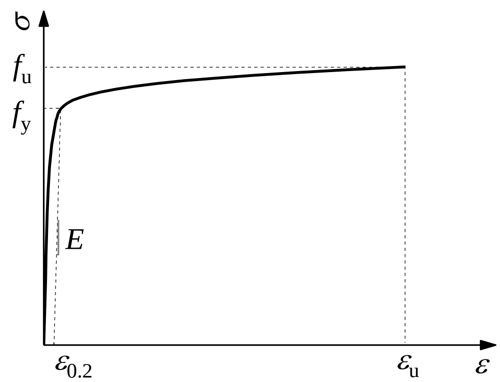

Fig. 15 Rounded stress-strain model for high-strength steel.

4.2 Proposed strain-rate effect model

It has been shown that the dynamic stress–strain response of steels is dependent on both strain rate and material strength, and can be characterized by multiplication of the stress in the static stress–strain curve by DIF_{avg}, as expressed by Eq. (5). A continuous model for DIF_{avg}, inspired by the C-S model (as shown in Eq. 1 [28]), but reflecting the dependency on both strain rate and yield strength, was therefore established in this study, based on the collected experimental results using least-squares regression. The resulting expression for DIF_{avg} is given by Eq. (13), where f_y is the yield strength in N/mm^2.

$$\mathrm{DIF}_{\mathrm{avg}}(\dot{\varepsilon}, f_{\mathrm{y}}) = 1 + \left(\frac{\dot{\varepsilon}}{D_{\mathrm{avg}}}\right)^{\frac{1}{p_{\mathrm{avg}}}} \tag{13}$$

where

$$D_{\mathrm{avg}} = 1000\left(\frac{f_{\mathrm{y}}}{235}\right)^{6} \tag{14}$$

and

$$p_{\mathrm{avg}} = 3\left(\frac{f_{\mathrm{y}}}{235}\right)^{0.2} \tag{15}$$

A corresponding expression for $\mathrm{DIF}_{\mathrm{y}}$ has also been newly established should there be a need for estimation of dynamic yield strength ($f_{\mathrm{y,d}}$), as given by Eq. (16). Fig. 16 shows the variation in $\mathrm{DIF}_{\mathrm{y}}$ and $\mathrm{DIF}_{\mathrm{avg}}$ values, determined according to the proposed models, with strain rate for two representative yield strengths——355 and 690 MPa. The strong dependency of $\mathrm{DIF}_{\mathrm{y}}$ and $\mathrm{DIF}_{\mathrm{avg}}$ on both strain rate and yield strength is clear. It is also clear that the $\mathrm{DIF}_{\mathrm{y}}$ values are larger than the $\mathrm{DIF}_{\mathrm{avg}}$ values, especially at high strain rates; this is consistent with the test results from both the present and previous studies.

$$\frac{f_{\mathrm{y,d}}}{f_{\mathrm{y}}} = \mathrm{DIF}_{\mathrm{y}} = 1 + \left(\frac{\dot{\varepsilon}}{D_{\mathrm{y}}}\right)^{\frac{1}{p_{\mathrm{y}}}} \tag{16}$$

where

$$D_{\mathrm{y}} = 1000\left(\frac{f_{\mathrm{y}}}{235}\right)^{3.8} \tag{17}$$

and

$$p_{\mathrm{y}} = 5\left(\frac{f_{\mathrm{y}}}{235}\right)^{-0.5} \tag{18}$$

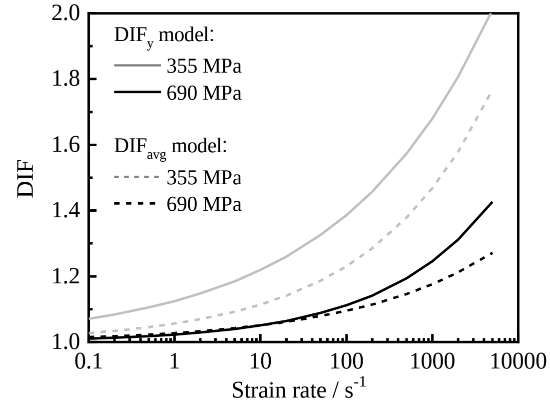

Fig. 16 Variation in DIF_y and DIF_{avg} values with yield strength and strain rate.

An overall comparison between the DIF_{avg} values obtained from the tests and the proposed DIF_{avg} model is shown in Fig. 17. The predicted values ($DIF_{avg,pred}$) using the proposed model and the measured values ($DIF_{avg,test}$) from the whole datasets are compared in Fig. 18a. The percentage prediction error (i.e., $(DIF_{avg,pred}-DIF_{avg,test})/DIF_{avg,test} \times 100\%$) was also calculated, and its distribution in the static yield strength and strain-rate space is plotted in Fig. 18b. The average value (Avg) of predicted to measured DIF_{avg} (i.e., $DIF_{avg,pred}/DIF_{avg,test}$) was found to be 1.00, with a standard deviation (St.D) of 0.07, demonstrating that the proposed model yields both accurate and consistent predictions. The prediction errors were less than 10% for 85% of the results, and only 13 data points (the red squares in Fig. 18) had errors exceeding 15%. These 13 data points were collected from five different studies, and there was no clear explanation for the observed deviations. Similar prediction accuracy was also observed for the DIF_y model (see Fig. 19), for which the Avg of the predicted to measured DIF_y was 1.00, with a St.D of 0.07.

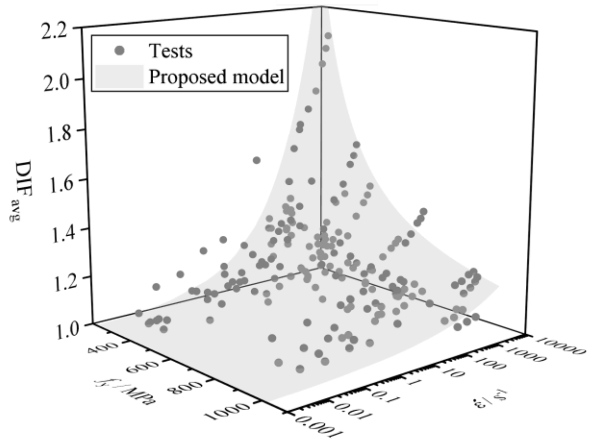

Fig. 17 Overall comparison between DIF_{avg} test results in the database and the proposed model.

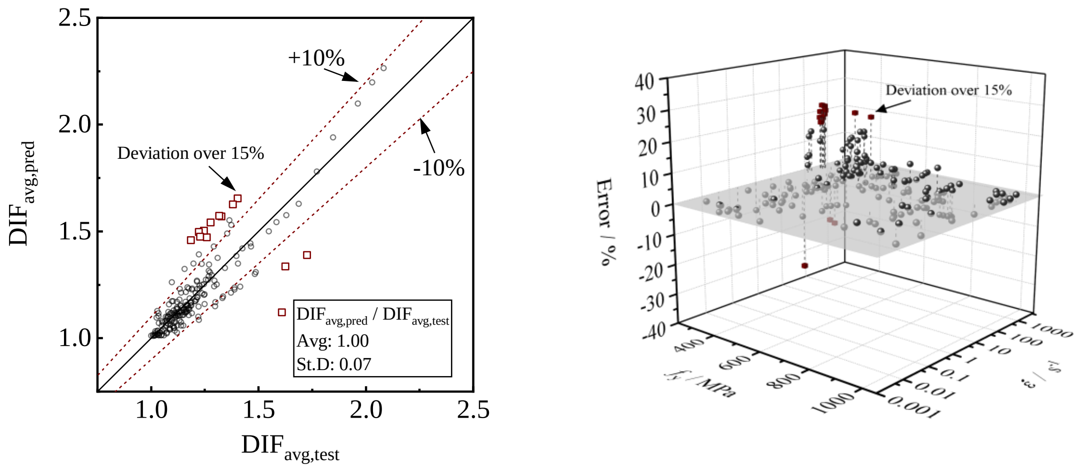

(a) Comparison of $DIF_{avg,pred}$ and $DIF_{avg,test}$ (b) Distribution of DIF_{avg} prediction error

Fig. 18 Comparison between test and predicted DIF_{avg} values.

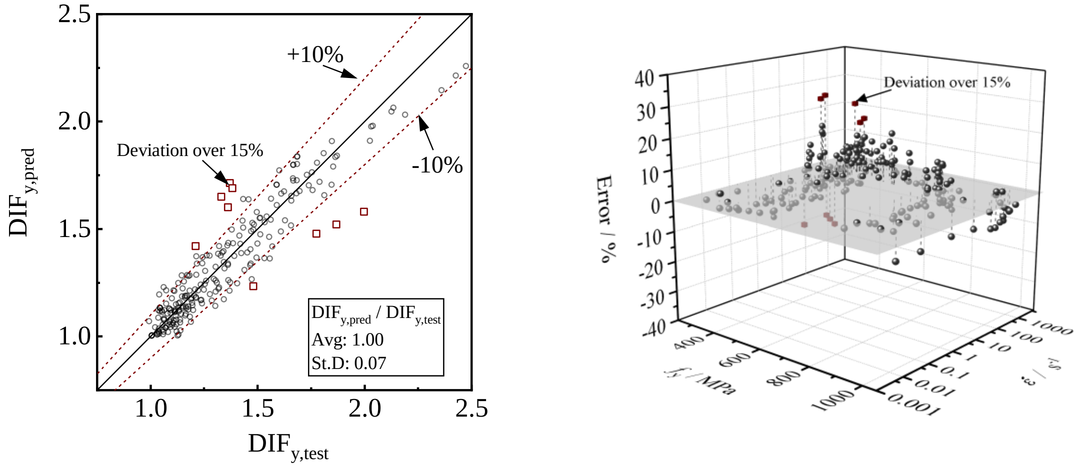

(a) Comparison of $DIF_{y,pred}$ and $DIF_{y,test}$ (b) Distribution of DIF_y prediction error

Fig. 19 Comparison between test and predicted DIF_y values.

Fig. 20 shows a detailed comparison between existing discrete models and proposed model, for each range of yield strength (similar yield strengths or grades). For conciseness, only one curve predicted by the proposed model is presented in each sub-figure, using the average yield strength for each range. The Avg of predicted to measured DIF_{avg} and the corresponding St.D are calculated, as summarized in Table 4. Generally higher accuracy of the proposed model can be seen from the comparisons. The Avg and St.D values for the existing models range from 1.00-1.24 and 0.03-0.52, respectively; while those of the proposed model range from 0.98-1.02 and 0.02-0.11, respectively. Hence, the proposed model has a wide range of applicability and provides a continuous relationship that reflects the dependency of DIF_{avg} on both the strain rate and material strength.

Some typical comparisons between measured and predicted dynamic stress–strain curves, illustrating the accuracy of the proposed model across a wide range of strain rates and steel grades, are also presented in Fig. 21.

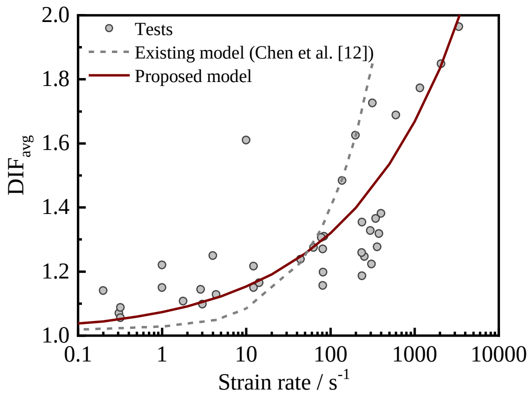

(a) f_y=235-342 MPa (e.g., Q235)

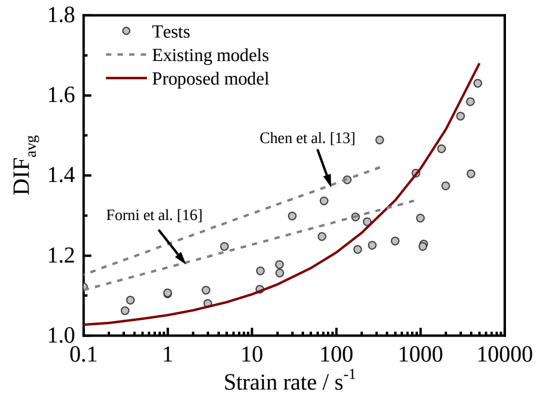

(b) f_y=358-416 MPa (e.g., Q345)

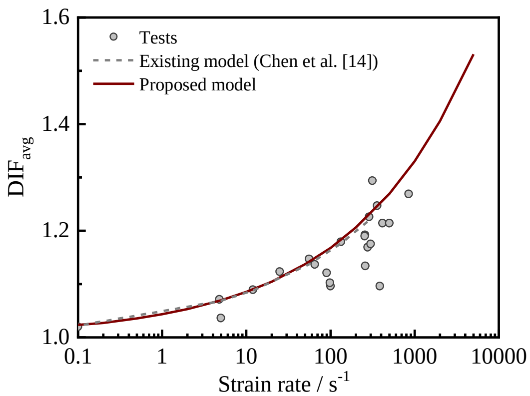

(c) f_y=427-441 MPa (e.g., Q420)

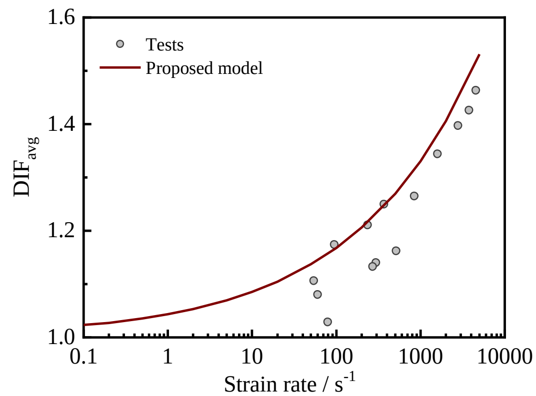

(d) f_y=467-516 MPa (e.g., Q460)

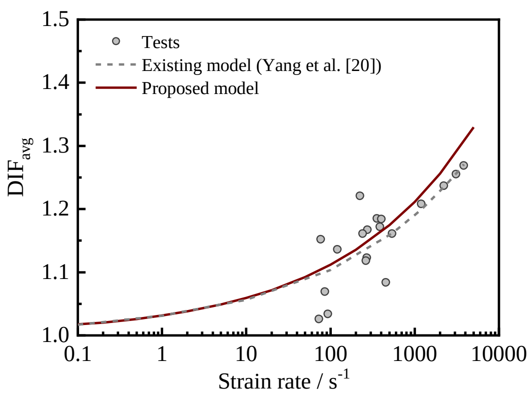

(e) f_y=578-636 MPa (e.g., Q550)

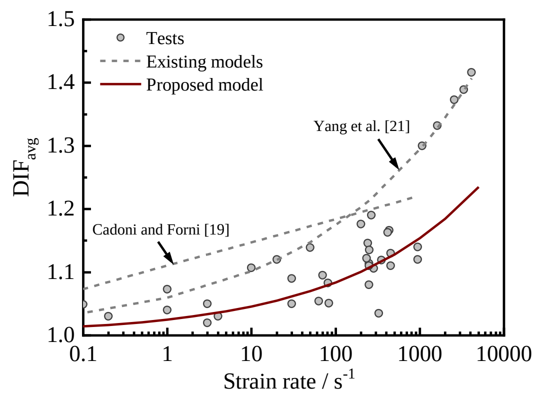

(f) f_y=727-817 MPa (e.g., S690)

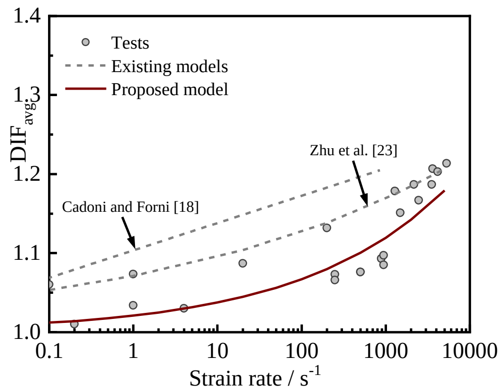

(g) f_y=906-1024 MPa (e.g., S890 and S960)

Fig. 20 Comparisons of tests, existing models and the proposed model.

Table 4 Comparison results for various models.

Tests			Existing Models			Proposed model	
f_y / MPa	$\dot{\varepsilon}$ /s^{-1}	Numbers of data	Models	Avg	St.D	Avg	St.D
235-342	0.01-5194	45	Chen et al. [12] for Q235	1.24	0.52	1.02	0.11
358-416	0.01-4813	36	Chen et al. [13] for Q345	1.08	0.07	0.99	0.08
			Forni et al. [16] for S355	1.02	0.07		
427-441	0.1-850	23	Chen et al. [14] for Q420	1.02	0.04	1.02	0.04
467-516	54-4562	14	\	\	\	1.01	0.04
578-636	73-3831	19	Yang et al. [20] for Q550	1.00	0.03	1.01	0.03
727-817	0.04-4109	39	Yang et al. [21] for S690	1.06	0.05	0.98	0.04
			Cadoni and Forni [19] for S690	1.05	0.06		
906-1024	0.04-5293	23	Zhu et al. [23] for S890	1.03	0.03	0.99	0.02
			Cadoni and Forni [18] for S960	1.06	0.04		
Summary:							
235-1024	0.01-5293	199	9 existing models	1.00-1.24	0.03-0.52	0.98-1.02	0.02-0.11

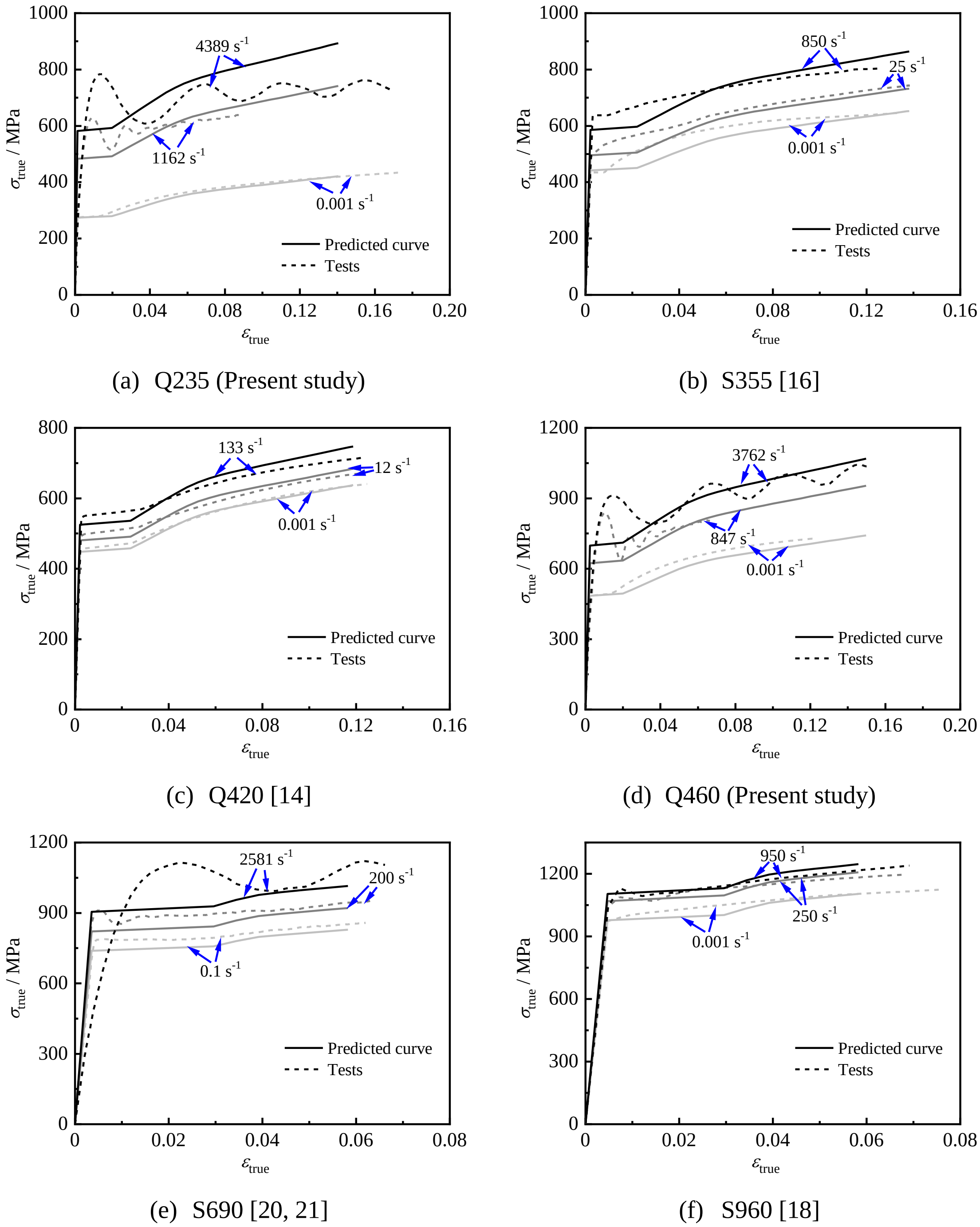

(a) Q235 (Present study)

(b) S355 [16]

(c) Q420 [14]

(d) Q460 (Present study)

(e) S690 [20, 21]

(f) S960 [18]

Fig. 21 Typical comparisons between measured and predicted dynamic true stress–strain curves.

For dynamic finite element and theoretical analyses, the true stress–strain relationship model of the steel is typically adopted. In actual applications for these dynamic analyses, the static stress–strain relationship model of the steel (for example, Eqs 6 and 7) should be transformed into the plastic true curve, and the strain-rate effect model (Eq. 13) should be multiplied to obtain its dynamic stress–strain relationship curve (Eq. 5).

5 Conclusions

A comprehensive investigation has been presented into the dynamic stress–strain properties of structural steel, featuring testing, the establishment of an experimental database and the development of a new constitutive model that depends on both strain rate and material strength. The conclusions of this study are as follows.

(1) SHPB tests on Q235, Q355, Q460, and S960 steels were conducted to obtain dynamic stress–strain curves at high strain rates and fill gaps in existing experimental datasets. The dynamic stress–strain curves and DIF_{avg} values, which quantify the average influence of strain rate over the full strain range, were obtained for each grade of steel.

(2) A database of 453 dynamic stress-strain curves was assembled, analysed and rationalised into 199 DIF_{avg} data points; the database was established from a combination of test results from the current study and existing test data collected from the literature. The strain-rate effect (i.e., DIF_{avg}) values were shown to increase with increasing strain rate but decrease with increasing yield strength.

(3) A continuous dynamic constitutive model was developed to predict the dynamic stress–strain curves of normal- and high-strength steels (up to 960 MPa) at intermediate and high strain rates (up to 5000 s^{-1}). The proposed model captures the combined influence

of strain rate and yield strength and is shown to provide an accurate description of the dynamic properties of structural steels, suitable for incorporation into advanced numerical simulations and parametric studies.

Acknowledgments

The authors are grateful for the financial support from the Heilongjiang Provincial Foundation for Distinguished Young Scholars (Grant No. JQ2021E003) and the National Natural Science Foundation of China (Grant No. 52078166). This work was also supported by the Startup Foundation of Scientific Research by Fuzhou University (Grant No. GXRC-20080), and the Fuzhou University Testing Fund of precious apparatus (Grant No. 2021T030).

References

[1] N. Jones, Structural Impact, Cambridge University Press, Cambridge, 2011.

[2] Wang J, Gardner L. Flexural buckling of hot-finished high-strength steel SHS and RHS columns. J Struct Eng 2017;143(6):04017028. DOI:10.1061/(ASCE)ST.1943-541X.0001763.

[3] Meng X, Gardner L. Testing, modelling and design of normal and high strength steel tubular beam-columns. J Constr Steel Res 2021;183:106735. https://doi.org/10.1016/j.jcsr.2021.106735.

[4] Meng X, Gardner L. Flexural buckling of normal and high strength steel CHS columns. Struct 2021;34:4364-75. https://doi.org/10.1016/j.istruc.2021.09.106.

[5] Manjoine MJ. The influence of rate of strain and temperature on the yield stresses of mild steel. J Appl Mech 1944;11:A-211.

[6] Cowell WL. Dynamic tests on selected structural steels. No. Ncel-Tr-642, Naval Civil Engineering Lab Port Hueneme Calif, 1969.

[7] Woodward RL, Brown RH. Dynamic stress-strain properties of a steel and a brass at strain rates up to 10^4 per second. Proc Ins Mech Eng 1975;189(1):107-15. https://doi.org/10.1243/PIME_PROC_1975_189_016_02.

[8] Haque MM, Hashmi MSJ. Stress-strain properties of structural steel at strain rates of up to 10^5 per second at sub-zero, room and high temperatures. Mech Mater 1984;3(3):245-56. https://doi.org/10.1016/0167-6636(84)90023-1.

[9] Langseth M, Lindholm US, Larsen PK, Lian B. Strain-rate sensitivity of mild steel grade St52-3N. J Eng Mech 1991;117(4):719-732. https://doi.org/10.1061/(ASCE)0733-9399(1991)117:4(719).

[10] Mirmomeni M, Heidarpour A, Zhao XL, Hutchinson CR, Packer JA, Wu C. Mechanical properties of partially damaged structural steel induced by high strain rate

loading at elevated temperatures – An experimental investigation. Int J Impact Eng 2015;76:178-88. https://doi.org/10.1016/j.ijimpeng.2014.10.001.

[11] Yu W, Zhao J, Shi J. Dynamic mechanical behaviour of Q345 steel at elevated temperatures: experimental study. Mater High Temp 2010;27(4):285-93. https://doi.org/10.3184/096034010X12761931945540.

[12] Chen J, Shu W, Li J. Experimental study on dynamic mechanical property of Q235 steel at different strain rate. J Tongji Univ (Natur Sci) 2016;44(7):1071-5. [in Chinese] https://doi.org/10.11908/j.issn.0253-374x.2016.07.014.

[13] Chen J, Shu W, Li J. Constitutive model of Q345 steel at different intermediate strain rates. Int J Steel Struct 2017;17(1):127-37. https://doi.org/10.1007/s13296-016-0122-8.

[14] Chen J, Li J, Li Z. Experiment research on rate-dependent constitutive model of Q420 steel. Constr Build Mater 2017;153:816-23. https://doi.org/10.1016/j.conbuildmat.2017.07.064.

[15] Alabi AA, Moore PL, Wrobel LC, Campbell JC, He W. Tensile behaviour of S690QL and S960QL under high strain rate. J Constr Steel Res 2018;150:570-80. https://doi.org/10.1016/j.jcsr.2018.08.009.

[16] Forni D, Chiaia B, Cadoni E. Strain rate behaviour in tension of S355 steel: Base for progressive collapse analysis. Eng Struct 2016;119:164-73. https://doi.org/10.1016/j.engstruct.2016.04.013.

[17] Luecke WE, McColskey JD, McCowan CN, Banovic SW, Fields RJ, Foecke T, et al. Mechanical properties of structural steels. National Institute of Standards and Technology, U.S. Department of Commerce, 2005: 79-99.

[18] Cadoni E, Forni D. Mechanical behaviour of a very-high strength steel (S960QL) under extreme conditions of high strain rates and elevated temperatures. Fire Safety J 2019;109:102869. https://doi.org/10.1016/j.firesaf.2019.102869.

[19] Cadoni E, Forni D. Strain-rate effects on S690QL high strength steel under tensile loading. J Constr Steel Res 2020;175:106348. https://doi.org/10.1016/j.jcsr.2020.106348.

[20] Yang H, Yang X, Varma AH, Zhu Y. Strain-rate effect and constitutive models for Q550 high-strength structural steel. J Mater Eng Perform 2019;28(11):6626-37. https://doi.org/10.1007/s11665-019-04431-2.

[21] Yang X, Yang H, Lai Z, Zhang S. Dynamic tensile behavior of S690 high-strength structural steel at intermediate strain rates. J Constr Steel Res 2020;168:105961. https://doi.org/10.1016/j.jcsr.2020.105961.

[22] Yang X, Yang H, Zhang S. Rate-dependent constitutive models of S690 high-strength structural steel. Constr Build Mater 2019;198:597-607. https://doi.org/10.1016/j.conbuildmat.2018.11.285.

[23] Zhu Y, Yang H, Zhang S. Dynamic mechanical behavior and constitutive models of S890 high-strength steel at intermediate and high strain rates. J Mater Eng Perform 2020;29:6727-39. https://doi.org/10.1007/s11665-020-05150-9.

[24] Comite Euro-International Du Beton (CEB). Concrete structures under impact and impulsive loading. Bulletin No.187, 1988;3.6.

[25] Chen L, Fang Q, Jiang X, Ruan Z, Hong J. Combined effects of high temperature and high strain rate on normal weight concrete. Int J Impact Eng 2015;86:40-56. https://doi.org/10.1016/j.ijimpeng.2015.07.002.

[26] Rao NRN, Lohrmann M, Tall L. Effect of strain rate on the yield stress of structural steel. ASTM J Mater 1966;1(1):684-737.

[27] Kassar M, Yu W. Effect of strain rate on material properties of sheet steels. J Struct Eng 1992;118(11):3136-50. https://doi.org/10.1061/(ASCE)0733-9445(1992)118:11(3136).

[28] Cowper G, Symonds PS. Strain hardening and strain rate effects in the impact loading of the cantilever beams, Technical Report No.28, Providence, RI: Brown University, Division of Applied Mathematics, 1957.

[29] Johnson GR, Cook WH. Fracture characteristics of three metals subjected to various strains, strain rates, temperatures and pressures. Eng Fract Mech 1985;21(1): 31-48.

[30] Zerilli FJ, Armstrong RW. Dislocation‐mechanics‐based constitutive relations for material dynamics calculations. J appl phys 1987;61(5):1816-25. https://doi.org/10.1063/1.338024.

[31] Mecking H, Kocks UF. Kinetics of flow and strain-hardening. Acta Metal 1981;29(11):1865-75. https://doi.org/10.1016/0001-6160(81)90112-7.

[32] Abaqus G. Abaqus 6.11. Dassault Systemes Simulia Corporation, Providence, RI, USA. 2011.

[33] ANSYS, ANSYS LS-DYNA. User guide, ANSYS. Inc. Version 15, 2017.

[34] Sun M, Packer JA. High strain rate behavior of cold-formed rectangular hollow sections. Eng Struct 2014;62:181-92. https://doi.org/10.1016/j.engstruct.2014.01.023.

[35] Yun X, Gardner L. Stress-strain curves for hot-rolled steels. J Constr Steel Res 2017;133:36-46. https://doi.org/10.1016/j.jcsr.2017.01.024.

[36] Gardner L, Yun X. Description of stress-strain curves for cold-formed steels. Constr Build Mater 2018;189:527-538. https://doi.org/10.1016/j.conbuildmat.2018.08.195.

[37] Yun X, Wang Z, Gardner L. Full-range stress-strain curves for aluminum alloys. J Struct Eng 2021;147(6):04021060. DOI: 10.1061/(ASCE)ST.1943-541X.0002999.